IET Generation, Transmission & Distribution

Research Article

IET Journals
The Institution of Engineering and Technology

Online assessment of voltage stability using Newton-Corrector algorithm

ISSN 1751-8687
Received on 1st August 2019
Revised 22nd May 2020
Accepted on 22nd June 2020
E-First on 16th July 2020
doi: 10.1049/iet-gtd.2019.1200
www.ietdl.org

Mazhar Ali[1] ✉, Elena Gryazina[1], Oleg Khamisov[1], Timur Sayfutdinov[1]

[1]Center for Energy Systems, Skolkovo Institute of Science and Technology, Moscow 143026, Russia

✉ *E-mail: mazhar.ali@skolkovotech.ru*

Abstract: The real-time robust and secure operation of power systems has become a challenging task, as the operating state evolves rapidly due to uncertainties associated with increasing renewable generation, less predictable loads, and various forms of contingencies. Therefore, an online voltage stability assessment is required to avoid any undesirable system behaviours or a large-scale blackout. Such evaluation is not just difficult but also computationally intensive mainly due to the continuously changing state of a grid. This study presents a numerically robust and fast algorithm for online voltage stability assessment with ease of implementation and programming. The proposed approach updates distance of voltage collapse in real-time by incorporating base-case collapse point solution and incoming data from measurement devices. Implementation of the proposed algorithm is described in detail, and its performance is validated on different IEEE test cases.

1 Introduction

Modern power systems are more vulnerable to instabilities as a result of operational proximity with their loadability limits [1–3]. Factors such as heavy loading conditions, uncertainties from renewable generation, load recovery dynamics, and different types of contingencies like line tripping or generator outages have made the secure operation of a grid challenging task [4–6]. In both planning and operational stages, network security is associated with voltage stability, which relates to the ability of the power system to maintain steady-voltage levels at all buses after being subjected to a disturbance [7–9]. Electrical grids experience voltage instability when the operating regime moves closer to voltage collapse or saddle-node bifurcation point, after which the real solution to power flow equations disappears [10–12]. Therefore, information about the margin of voltage collapse is necessary for better security assessment. Also, this information can be useful to considerably decrease the chances of power disruption and provide informed control actions for the robust and secure operation of a grid [13, 14].

Voltage instability is a well-recognised phenomenon in the power system community as it prompted many cascading events and blackouts in past years [15–17]. Disruptions leading up to voltage instability incidents are usually triggered by the continuous rise of loads or significant change of the network topology following a critical contingency. Consequently, voltage stability is categorised as a small or a large disturbance stability problem based on the nature of disruption. Furthermore, based on the time scale of interest, the cause of a potential voltage instability can be grouped into short-term and long-term phenomena [18]. The scope of this paper is focused on the long-term voltage behaviour in power systems.

Recently, reported voltage outages in Asia, Europe, and the US have given thrust for developing effective computational tools for the voltage stability analysis. Studies are performed to validate the feasibility of an operating regime at any given time, by calculating its proximity to collapse. Traditional approaches fall into two broad categories. The first kind uses voltage stability index (VSI), a scalar parameter that can be monitored as network state changes over time [1, 19]. Index-based methods are simple, computationally tractable, and provide a notion of instability; however, these methods are not suitable for precautionary measures [20]. In contrast to the index-based methods, the continuation techniques like in [21, 22], and direct methods from [12, 23] provide a quantitative bound on the distance to collapse in the parameter space (like voltage setpoints or power injections). The algorithmic procedure described in this paper belongs to the latter category.

Voltage stability studies have been approached with both static and dynamic interpretations. The static analysis employs a steady-state model based on power flow equations to estimate security margin from voltage collapse [24, 25]. In contrast, the dynamic analysis considers a set of non-linear differential-algebraic equations to model voltage fluctuations at each bus in time following some disturbances [25]. Although the stability problem is dynamic by nature, the effects of system dynamics from long-term phenomena are usually slow [18, 26]. Therefore, we propose to use a steady-state model, which is also extensively used by industry. However, it is worth highlighting that the proposed approach does not account for all processes within the grid, i.e. changing load caused by on-load tap changers (OLTCs) and over excitation limiters (OELs).

Moreover, voltage stability assessment can be performed either online or offline mode. The online studies rely on real-time measurements from the phasor measurement unit (PMU) or supervisory control and data acquisition (SCADA) devices, and updates margin of voltage collapse for moving the state of a network [27]. It also assists the transmission system operator (TSO) to determine acceptable manoeuvrability for an operating regime, and a decision on optimum preventive measures, such as reactive power dispatch rescheduling, switching capacitor banks, and load shedding [28]. Contrary, offline analysis is usually adopted for planning purposes like grid expansion studies and allocation of reactive power reserves. From the computational perspective, offline studies have no constraint on computational time. Contrarily, the online studies have a significant computational time constraint such that all the incoming measurements can be processed for real-time assessment [27, 29]. This paper is focused on online voltage stability assessment based on information provided by PMUs or a SCADA system.

Over the years, several efforts have been made to this problem. As mentioned earlier, contributions fall into two main classes. The first type of methods is based on the sensitivity indices or VSI, as reported in [24, 30]. Normally, a static or quasi-static model assumption is used to make these stability indices, which provide local indicators of instability at each bus in the network. The authors of [27, 31–33] and follow-up works from [34–38] propose indices based on the load flow Jacobian and through phasor

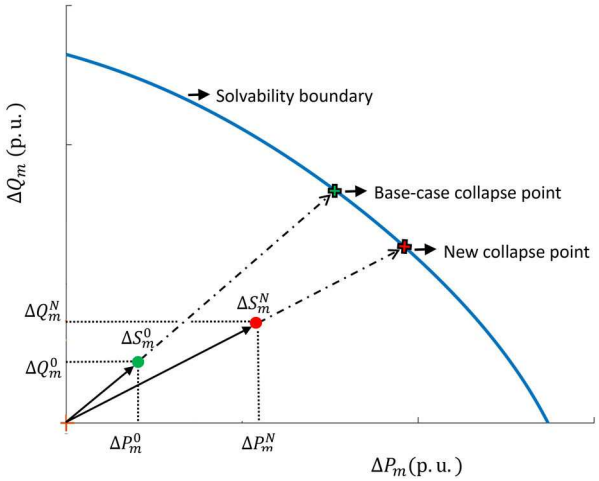

Fig. 1 *Solvability boundary in $\Delta P_m\,\Delta Q_m$ space*

information available at PMUs, respectively. In [39], a real-time PMU-based index is given through the maximum loading capacity of a bus combined with the Thevenin equivalent theory for aggregated representation. Recently, an innovative neural network strategy is also being used for such methods in [40, 41]. A trained neural network predicts the instability through an index at each bus by incorporating power flow solutions and incoming data from PMUs. Neural network approaches are beneficial in the long run for a better understanding of the system behaviour. Despite the simplicity in implementation and computational speed, index-based methods fail to provide a quantitative assessment needed to avoid an imminent contingency.

In the second category of methods, several algorithms have been suggested that provide a quantitative bound or margin in power injection space to assess the distance to instability. The notable contributions are based on continuation power flow (CPF) from [21, 22]. Continuation methods are equitably accurate but suffer from the longer computational time since these techniques depend on repetitive power flow calculations. Recently published Holomorphic Embedding Load Flow Method (HELM) provides a fast and reliable way to compute stability margins [42, 43]. However, its accuracy is sensitive to good germ and order of approximation in the power series [42]. While the recent works from [12, 44] supplement effort focused on the direct computation of the distance to collapse, some estimate based approaches for online purposes are also reported in [29, 45]. Demerits of the above mentioned methods are linked to either computational speed, convergence, scalability to large cases, and the computational time. They might not be attractive for online purposes. Finally, some of these algorithms also require a reformulation of the standard power flow model, which results in a difficult implementation.

In this work, we propose a novel algorithm that updates the margin of voltage collapse in real-time, incorporating information about a base-case collapse point and incoming data from measurement PMUs or SCADA system. The proposed approach is referred to as the Newton-Corrector (NC) algorithm. Unlike CPF solvers, it does not require an explicit tracking of the solution manifold. The mathematical structure of the NC algorithm extends the system of power flow equations using an additional equation to characterise solutions on the boundary of solvability. This auxiliary condition is denoted as the parametric equation throughout this paper. Three different versions of the parametric equation are formulated, which provides sufficient freedom to change the voltage on sensitive buses, do not allow any unexpected numerical updates. The algorithm enables a fast evaluation of the margin to collapse for each new state of a grid, with precision and ease of implementation from the computational context. Also, it does not require a reformulation of the power flow equations. Finally, the performance of the proposed algorithm has been demonstrated in a number of standard scenarios. The key contributions of this work are organised as follows:

i. The proposed approach updates the distance of voltage collapse in real-time by incorporating base-case collapse point solution and incoming data from measurement devices.
ii. The proposed algorithm is fast and numerically robust for online voltage stability.
iii. Avoiding the need to reformulate power flow equations, the proposed approach ensures ease of implementation and programming.

The paper is organised as follows. Section 2 describes the problem statement from geometrical interpretations. Section 3 presents the general mathematical formulation and system of equations. Details about the base-case collapse point solution are addressed in Section 4. The mathematical structure of the proposed NC algorithm and relevant parametric equations are given in Section 5. In Sections 6 and 7, we describe the implementation and results from different test cases, respectively. Finally, the conclusion and future plans are provided in Section 8.

2 Problem statement

The boundedness of power injection space is portrayed in Fig. 1. The solid curve depicts a solvability boundary in ΔP_m (active power injection) and ΔQ_m (reactive power injection) space. Here, index 'm' indicates a random bus in the network. The solvability boundary encloses a set of operating points in $\Delta P_m\,\Delta Q_m$ for which the real-valued solution of power flows exist. Any operation beyond this boundary will result in voltage collapse. Hence, quantifying the distance of voltage collapse is crucial for security assessment [46]. As the TSO can determine the relative degree of security for an operating regime, acceptable manoeuvrability if it changes, and optimal control measures needed to bring it within a feasible region of operation [46, 47].

In a conventional setting, system operating state is defined by a complex vector as

$$\Delta S_m = \Delta P_m + j\Delta Q_m\,. \tag{1}$$

For security assessment, as mentioned before, the feasibility of any state ΔS_m is evaluated by its margin to solvability boundary. Let us assume two distinct operating states ΔS_m^0 and ΔS_m^N as shown in Fig. 1. The base-case state ΔS_m^0 is a real-time state estimation of a pre-contingency case, or future postulated system condition [48]. It is defined on an hourly basis. And serves as a benchmark regime to build power flows, transmission flows, or transfer capability calculations. The point on the solvability boundary corresponding to ΔS_m^0 is referred to as 'base-case collapse point'. In real-time, the state of the network changes on a continuous manner after every few seconds denoted by ΔS_m^N, and the corresponding point on solvability boundary is referred to as 'new collapse point'. It can be observed that even in the close vicinity with the base-case, the margin to a new collapse point for ΔS_m^N might be significantly smaller.

The goal of this study is to develop an algorithm to update the margin to collapse for continuously changing state ΔS_m^N without significant computational effort, by exploiting the base-case collapse point and incoming measurements. First, a general mathematical structure is given in the next section.

3 Mathematical formulation

To investigate the voltage stability problem from the context of long-term stability phenomenon, a static model of the power system is considered in this study. The classical non-linear algebraic system of equations is presented in a compact form as

$$f_i^N(x,\lambda) = f_i(x) - \lambda\Delta S_i^N = 0, \quad i = 1,2,\ldots,n\,. \tag{2}$$

Here f_i^N: $\mathbb{C}^n \times \mathbb{C} \to \mathbb{C}^n$ denotes n number of power flow equations with $\boldsymbol{x} \in \mathbb{C}^n$ vector of system variables, while $\lambda \in \mathbb{R}$ represents the

loadability parameter. In (2), $\Delta S_i^N \in \mathbb{C}^n$ denotes the new operating state of the grid in real time, i.e. $\Delta S_i^1, \Delta S_i^2, \Delta S_i^3, \ldots$. The new state ΔS_i^N is determined by analysing incoming data from measurement devices installed in the network, combined with the measurement pre-processing by a state estimator, etc. [20].

For a given operating state ΔS_i^N, the loadability parameter λ satisfies the following condition $1 \leq \lambda \leq \lambda_{\max}$. For $\lambda = 1$, the solution of (2) describes a normal power flow. While for $\lambda = \lambda_{\max}$, the solution of (2) corresponds to the voltage collapse, equivalently $\lambda_{\max}$ describes the margin of ΔS_i^N to the voltage collapse. The online voltage stability assessment requires solving (2) in real time for each new operating regime ΔS_i^N to calculate corresponding $\lambda_{\max}$, which is a computationally intensive task.

The framework of this paper is focused on developing a computationally fast algorithm that can solve (2) faster for each new operating state ΔS_i^N in time by utilising the solution of (2) for a base-case regime ΔS_i^0 along with the measurements from PMU devices. Details about the system of equations and variables considered

3.1 Modelling of power flows

The set of equations considered in (2) is only power flows. The power flow model can be described in both polar and rectangular coordinates. The reason to choose a formulation in polar coordinates is twofold. (i) First, it is easier to implement and to program. (ii) Second, it contains less equations and variables compared to the rectangular formulation. Finally, it preserves the sparse structure of the power flow model.

The complex voltage phasor at each bus i is represented by the polar coordinates

$$\hat{V}_i = \left|V_i\right| \angle \theta_i \tag{3}$$

This way the power flows in (2) can be stated as follows:

$$f_i^N(x, \lambda) = \hat{V}_i \sum_{k=1}^{n} (\hat{Y}_{i,k} \hat{V}_k)^* - \lambda \Delta S_i^N \quad = 0 \tag{4}$$

In (4), $\hat{Y}_{i,k}$ defines the complex entries of the admittance matrix $\boldsymbol{Y}_{\text{bus}} \in \mathbb{C}^{n \times n}$, while ΔS_i^N is expressed in terms of active and reactive power injections

$$\Delta S_i^N = (P_{\text{gen},i}^N - P_{\text{load},i}^N) + \boldsymbol{j}(Q_{\text{gen},i}^N - Q_{\text{load},i}^N) \tag{5}$$

In an n bus system, $\mathcal{N} = \{1, 2, \ldots, n\}$ represents the set of all buses, $\mathcal{L}$ is the set of load (PQ) buses, and $\mathcal{G}$ is the set of generator (PV) buses. For each bus $i \in \mathcal{N}$ in the network except slack bus $\mathcal{S}$, one can write (4) explicitly in terms of real and reactive power balance as

$$\left|V_i\right| \sum_{k=1}^{n} \left\{ \left|V_k\right| \left(G_{i,k} \cos(\theta_i - \theta_k) + B_{i,k} \sin(\theta_i - \theta_k)\right) \right\} - \lambda (P_{\text{gen},i}^N - P_{\text{load},i}^N) = 0 \tag{6}$$

$$\left|V_i\right| \sum_{k=1}^{n} \left\{ \left|V_k\right| \left(G_{i,k} \sin(\theta_i - \theta_k) - B_{i,k} \cos(\theta_i - \theta_k)\right) \right\} - \lambda (Q_{\text{gen},i}^N - Q_{\text{load},i}^N) = 0 \tag{7}$$

In (6) and (7), both active and reactive generations at bus i are denoted by $P_{\text{gen},i}^N$ and $Q_{\text{gen},i}^N$ respectively, likewise active and reactive loads are $P_{\text{load},i}^N$ and $Q_{\text{load},i}^N$. $|V_i|$ and $|V_k|$ are the voltage magnitudes at the ith and kth buses of a network. The terms $G_{i,k}$ and $B_{i,k}$ represent the real and imaginary entries of the admittance matrix as $\hat{\boldsymbol{Y}}_{ik} = G_{i,k} + \boldsymbol{j}B_{i,k}$.

To summarise, a set of equations considered in (2) are (6) and (7) for every PQ bus, while only (6) for every PV bus in the network. Consequently, the system of variables in (2) consists of phase angle θ_i for every PQ and PV bus, and voltage magnitude $|V_i|$ for only PQ buses in the system.

4 Base-case collapse point

To solve the system in (2) for each new operating state ΔS_i^N, it is required to calculate the margin to collapse for a base-case regime ΔS_i^0. The base-case collapse point solution sets the foundation for the proposed methodology in this paper.

$$f_i^0(x, \lambda) = f_i(x) - \lambda \Delta S_i^0 = 0, \quad i = 1, 2, \ldots, n \tag{8}$$

The general mathematical intuition of (8) is conceptually similar to one in (2) except it is stated for a base-case regime ΔS_i^0. The set of equations in (8) is underdetermined as there are '$n + 1$' variables with only 'n' equation, thus solution of (8) describes a 1-manifold curve. To solve the problem deterministically, it is possible to parameterise the solution manifold with λ and use continuation based techniques as proposed in [21]. The continuation algorithms are well explored and robust for tracing the solution space curves but requires a lot of computational effort which may not be attractive for online voltage stability problem [49]. An alternative way, to solve (8) is based on the direct methods for determining the margin to collapse without explicit tracking of the solution manifold as explored in [12]. To solve (8) for $\lambda_{\max}$, the proposed direct algorithm from [12] extends the system in (8) with an additional equation referred as 'transversality condition'. This condition describes the degeneracy of the Jacobian $\boldsymbol{J}^0 = \partial f_i^0 / x_j$. Thus, the extended system can be written as

$$f_i^0(x, \lambda) = 0, \quad i = 1 \ldots n \tag{9a}$$

$$g(x) = 0 \tag{9b}$$

Here $g(x)$ denotes the degeneracy of $\boldsymbol{J}^0$ and there are several ways to enforce this condition as described in [12]. The most common and obvious choice is determinant but it suffers from numerical instabilities and also not scalable for the large test cases [50]. Several possible choices for $g(x)$ either based on vector or scalar conditions are presented in [12]. In the next section, we consider two distinct options for $g(x)$ which will form the basis for NC algorithm proposed in this paper.

4.1 Eigenvector-based condition

The most common way to enforce $g(x)$ is based on a eigenvector transversality condition [10, 12]. In this choice, the degeneracy of $\boldsymbol{J}^0$ is enforced by introducing a normalised eigenvector $\boldsymbol{y}^0$ corresponding to zero eigenvalue as

$$g_{\text{eig}}(x, y) = \begin{bmatrix} \boldsymbol{J}^0 \boldsymbol{y}^0 \\ \boldsymbol{y}^{0\top} \boldsymbol{y}^0 - 1 \end{bmatrix} \tag{10}$$

Equation (10) enforces a non-trivial kernel, i.e. $\boldsymbol{J}^0$ is degenerate such that $\boldsymbol{y}^0$ is the normalised right eigenvector with zero eigenvalue [12]. The right eigenvector $\boldsymbol{y}^0$ preserves information about the sensitivity of buses in the form of voltage magnitudes and phase angles. The condition g_{eig} can also be stated for the corresponding left eigenvector $\boldsymbol{z}^0$ as

$$g_{\text{eig}}(x, z) = \begin{bmatrix} \boldsymbol{J}^{0\top} \boldsymbol{z}^0 \\ \boldsymbol{z}^{0\top} z - 1 \end{bmatrix} \tag{11}$$

The interpretation of the above condition is equivalent to (10) except its formulated for the left eigenvector $\boldsymbol{z}^0$. However, unlike

$\boldsymbol{y}^0$, the left eigenvector $\boldsymbol{z}^0$ preserves information about the sensitive directions for active and reactive power injections.

4.2 Singular value-based condition

Here, the system in (9) is complemented by a scalar transversality condition based on the smallest singular value of $\boldsymbol{J}^0$. For singular value decomposition, $\boldsymbol{J}^0 = \boldsymbol{U}^0\boldsymbol{\Sigma}^0(\boldsymbol{V}^0)^\top$ is the matrix, $\boldsymbol{U}^0$ and $\boldsymbol{V}^0$ are the orthogonal matrices, respectively. While $\boldsymbol{\Sigma}^0$ is the diagonal matrix consisting of singular values in the following order $\sigma_1^0 > \sigma_2^0 > \cdots > \sigma_n^0 \geq 0$. At the voltage collapse point $\boldsymbol{J}^0$ becomes degenerate and therefore the nth singular value becomes equal to zero. Therefore, $g(x)$ can be stated as follows:

$$g_{\text{svd}}(x) = \sigma_n^0 \qquad = \boldsymbol{u}_n^{0\top}\boldsymbol{J}^0\boldsymbol{v}_n^0 \tag{12}$$

From (12) σ_n^0 is the nth singular value, while $\boldsymbol{u}_n^0$ and $\boldsymbol{v}_n^0$ represent the normalised nth left and right singular vectors, respectively, [12]. Here σ_n^0 is a measure of system proximity to voltage collapse. The nth right singular vector $\boldsymbol{v}_n^0$ indicates the sensitive voltages and phase angles. While the nth left singular vector $\boldsymbol{u}_n^0$ describes the most sensitive directions for active and reactive power injections.

The margin of voltage collapse for new operating points $\Delta S_i^1, \Delta S_i^2, \ldots$ can be calculated in the real time with a small computational effort by utilising the solution of (9) for the base-case with addition of real-time measurements as explained in the next section.

5 NC algorithm

The main goal is to update the collapse point information as an operating state of a network moves from the base-case ΔS_i^0 to new state ΔS_i^N. One can use information from the base-case collapse point to avoid additional computational time. Following the notation from (2) there are 'n' number of equations with '$n+1$' variables. Thus, a parametric equation is devised as an additional condition to solve for '$n+1$' unknowns. The generalised form for the system of equations can be written as

$$f_i^N(x,\lambda) \;= 0, \quad i = 1, \ldots, n \tag{13a}$$

$$p(x(s),\lambda(s)) \;= 0 \tag{13b}$$

Here s denotes the parameterisation of the solution manifold. The condition $p(x,\lambda)$ can be interpreted as a corrector equation, which enforces solution of (2) on the solvability boundary using the information about the non-trivial kernel of $\boldsymbol{J}^0$. The choice of parameterisations is formulated through the conditions described in the previous section; more details regarding $p(x,\lambda)$ are given in the subsequent sections. Numerical solution of (13) can be obtained using traditional Newton iterations in the space of x and λ. Therefore, the proposed method is referred to as Newton-Corrector (NC) algorithm. We can describe iteration steps as follows:

$$f^N + (\partial_x f^N)\Delta x + (\partial_\lambda f^N)\,\Delta\lambda = 0 \tag{14a}$$

$$p + (\partial_x p)^\top \Delta x + (\partial_\lambda p)\Delta\lambda = 0 \tag{14b}$$

The inflated system Jacobian will be non-singular

$$\mathcal{J} = \begin{bmatrix} \partial_x f & \partial_\lambda f \\ \partial_x p & \partial_\lambda p \end{bmatrix} \tag{15}$$

The next correction x' and λ' in the Newton iteration is then computed as follows:

$$x' = x + \alpha\Delta x \tag{16a}$$

$$\lambda' = \lambda + \alpha\Delta\lambda \tag{16b}$$

Here α denotes the Newton step size [51]. Normally, α is chosen to be small enough to ensure global convergence of the NC algorithm. Iterations will continue until a solution with the desired precision level is achieved. In general, problem for updating the margin to collapse for ΔS_i^N can be summarised as

i. Updating the collapse point information in real-time with incoming measurements from PMUs combined with a measurement pre-processing by a state estimator.
ii. Calculating updated collapse point after system experiences some intermittent disturbances like generator or transmission line outages.

In principle, both scenarios are conceptually similar, as in either case, the state of a grid moves from ΔS_i^0 to ΔS_i^N. One key difference is the margin to collapse between the base-case and the updated state. In the first scenario, this margin is somewhat smaller in comparison to the second case.

For either one of the scenarios described above, the NC algorithm can be used to find a solution. The system in (13) is solved using standard Newton iterations with a proper selection of the parameterisation having a base-case collapse point as an initial starting point. Selection of the parametric equation $p(x,\lambda)$ should be made in a way that; (i) it allows maximum flexibility for 'from the bus' and 'to the bus' to make large updates during the iteration process, (ii) and also provides sufficient freedom to change the voltage on sensitive buses without compromising the numerical stability of the algorithm. In the next sections, we drive three different versions of the parametric equation from the non-trivial kernel of a base-case Jacobian $\boldsymbol{J}^0$.

5.1 Parameterisation: first choice

For new operating directions ΔS_i^N, one can take advantage of the base-case solution defined by (10) and (11). Let's assume that ΔS_i^N is just a slightly perturbed ΔS_i^0 such that

$$\boldsymbol{J}^N = \boldsymbol{J}^0 + \delta\boldsymbol{J} \tag{17}$$

In (17), $\boldsymbol{J}^N$ is the Jacobain associated with ΔS_i^N. While $\delta\boldsymbol{J}$ is the change between $\boldsymbol{J}^N$ and $\boldsymbol{J}^0$. We introduce a small perturbation parameter ϵ in (17) to calculate eigenvalues Λ_i of $\boldsymbol{J}^N$ as a function of eigenvalue decomposition of $\boldsymbol{J}^0$.

$$\boldsymbol{J}^N = \boldsymbol{J}^0 + \epsilon\delta\boldsymbol{J} \tag{18}$$

Let's calculate the first-order approximation to the corresponding eigenvalues Λ_i of $\boldsymbol{J}^N$,

The eigenvalue equation yields

$$\boldsymbol{J}^N\boldsymbol{y}_i = \Lambda_i\boldsymbol{y}_i \tag{19}$$

Here $\boldsymbol{y}_i$ is right equivocator for $\boldsymbol{J}^N$. As ϵ is a small parameter, we shall expand the solution of (19) as a Taylor series in ϵ,

$$\begin{aligned}(\boldsymbol{J}^0 + \epsilon\delta\boldsymbol{J})(\boldsymbol{y}_i^0 + \epsilon\boldsymbol{y}_i^1 + \epsilon^2\boldsymbol{y}_i^2, \ldots) \\ = (\Lambda_i^0 + \epsilon\Lambda_i^1 + \epsilon_i^2\Lambda_i^2, \ldots)(\boldsymbol{y}_i^0 + \epsilon\boldsymbol{y}_i^1 + \epsilon^2\boldsymbol{y}_i^2, \ldots)\end{aligned} \tag{20}$$

For ϵ^0,

$$\boldsymbol{J}^0\boldsymbol{y}_i^0 = \Lambda_i^0\boldsymbol{y}_i^0, \tag{21}$$

For ϵ^1,

$$\boldsymbol{J}^0\boldsymbol{y}_i^1 + \delta\boldsymbol{J}\boldsymbol{y}_i^0 = \Lambda_i^0\boldsymbol{y}_i^1 + \Lambda_i^1\boldsymbol{y}_i^0 \tag{22}$$

Multiplying both sides with $z_i^{0\top}$ left eigenvector corresponding to Λ_i^0 of $\boldsymbol{J}^0$,

$$z_i^{0\top}\boldsymbol{J}^0\boldsymbol{y}_i^1 + z_i^{0\top}\delta\boldsymbol{J}\boldsymbol{y}_i^0 = \Lambda_i^0 z_i^{0\top}\boldsymbol{y}_i^1 + \Lambda_i^1 z_i^{0\top}\boldsymbol{y}_i^0 \tag{23}$$

Here, $z_i^{0\top}\boldsymbol{J}^0\boldsymbol{y}_i^1 = \Lambda_i^0 z_i^{0\top}\boldsymbol{y}_i^1$ thus,

$$\Lambda_i^1 = \frac{z_i^{0\top}\delta\boldsymbol{J}\boldsymbol{y}_i^0}{z_i^{0\top}\boldsymbol{y}_i^0} \tag{24}$$

Thus, the first-order approximation to Λ_i as a function of λ_i^0, $\boldsymbol{y}_i^0$ and z_i^0 can be written as follows:

$$\Lambda_i = \Lambda_i^0 + \frac{z_i^{0\top}\delta\boldsymbol{J}\boldsymbol{y}_i^0}{z_i^{0\top}\boldsymbol{y}_i^0} \tag{25}$$

Now let's assume $\boldsymbol{J}^0$ is degenerate, and the ith eigenvalue Λ^0 is zero. Then, according to (10) and (11), z^0 and $\boldsymbol{y}^0$ represent the normalised left and right null space eigenvectors of $\boldsymbol{J}^0$. Thus, for $\boldsymbol{J}^N$ to be degenerate at the solvability boundary the corresponding ith eigenvalue Λ should be equal to zero as well. Hence, parametric equation for the smallest eigenvalue of $\boldsymbol{J}^N$ can be formulated as

$$p_{\text{eig}}(\boldsymbol{y}^0, z^0) = z^{0\top}\boldsymbol{J}^N\boldsymbol{y}^0 \tag{26}$$

To summarise, one can solve the following system of equations for new operating regime assuming that the normalised left and right eigenvectors corresponding to null space of $\boldsymbol{J}^0$ are known.

$$f_i^N(x,\lambda) = 0, \quad i = 1\ldots n \tag{27a}$$

$$p_{\text{eig}}(\boldsymbol{y}^0, z^0) = 0, \tag{27b}$$

5.2 Parameterisation: second choice

In this section, we formulate another parametric equation p_{svd} based on the base-case solution defined by (12). Following the same assumption that ΔS_i^N is just slightly perturbed ΔS_i^0 such that

$$\boldsymbol{J}^N = \boldsymbol{J}^0 + \delta\boldsymbol{J} \tag{28}$$

Introducing a perturbation parameter ϵ in (28) to solve for singular values σ_i of $\boldsymbol{J}^N$.

$$\boldsymbol{J}^N = \boldsymbol{J}^0 + \epsilon\delta\boldsymbol{J} \tag{29}$$

The singular value decomposition yields

$$\boldsymbol{u}_i^\top\boldsymbol{J}^N\boldsymbol{v}_i = \sigma_i \tag{30}$$

Here $\boldsymbol{u}_i$ and $\boldsymbol{v}_i$ correspond to the ith left and right singular vectors of $\boldsymbol{J}^N$. Similar to the previous section, we shall expand the solution (30) as a Taylor series in ϵ.

$$\begin{aligned}(\boldsymbol{u}_i^{0\top} + \epsilon\boldsymbol{u}_i^{1\top} + \epsilon^2\boldsymbol{u}_i^{2\top} + \cdots)(\boldsymbol{J}^0 + \epsilon\delta J)(\boldsymbol{v}_i^0 + \epsilon\boldsymbol{v}_i^1 \\ + \epsilon^2\boldsymbol{v}_i^2 + \cdots) = (\sigma_i^0 + \epsilon\sigma_i^1 + \epsilon^2\sigma_i^2 + \cdots)\end{aligned} \tag{31}$$

After some algebraic manipulation the first-order approximation of the ith singular value σ_i of $\boldsymbol{J}^N$ can be written as a function of σ_i^0, $\boldsymbol{u}_i^0$ and $\boldsymbol{v}_i^0$ as follows:

$$\sigma_i = \sigma_i^0 + \boldsymbol{u}_i^{0\top}\delta\boldsymbol{J}\boldsymbol{v}_i^0 \tag{32}$$

At solvability boundary, $\boldsymbol{J}^0$ is degenerate and the nth singular value σ_n^0 is zero. Then, according to (12), $\boldsymbol{u}_n^0$ and $\boldsymbol{v}_n^0$ are the normalised left and right nth singular vectors corresponding to the null space of $\boldsymbol{J}^0$. For $\boldsymbol{J}^N$ to be degenerate the nth singular value should be equal to zero. Thus, the second parameterisation p_{svd} becomes

$$p_{\text{svd}}(\boldsymbol{u}_n^0, \boldsymbol{v}_n^0) = \boldsymbol{u}_n^{0\top}\boldsymbol{J}^N\boldsymbol{v}_n^0 \tag{33}$$

One can solve the following system of equations for ΔS_i^N assuming that the left and right singular vectors corresponding to non-trivial kernel of $\boldsymbol{J}^0$ are known.

$$f_i^N(x,\lambda) = 0, \quad i = 1,\ldots,n \tag{34a}$$

$$p_{\text{svd}}(\boldsymbol{u}_n^0, \boldsymbol{v}_n^0) = 0 \tag{34b}$$

Conceptually, the formulations of the proposed parametric conditions, i.e. p_{eig} and p_{svd} are similar.

5.3 Parameterisation: third choice

A rather simple but effective parametric equation was introduced in [49]. The base-case collapse condition from (12) preserves information about the bus sensitivity in a network. The nth right singular vector $\boldsymbol{v}_n^0$ from (12) can provide sensitivity of buses in terms of system variables. All the entries in the $\boldsymbol{v}_n^0$ are positive. If the ith entry of $\boldsymbol{v}_n^0$ is close to zero, than corresponding ith bus is less sensitive and vice versa if the ith entry of $\boldsymbol{v}_n^0$ is large. From a complex notation, the real part of vector $\boldsymbol{v}_n^0$ relates to sensitivity in terms of phase angles, while the imaginary part links to sensitivity of buses in the form of voltage magnitudes. Therefore, a parametric equation based on $\boldsymbol{v}_n^0$ is well suited here. The proposed equations p_{s} can be expressed as follows:

$$p_{\text{s}}(\boldsymbol{v}_n^0) = \sum_{k=1}^{n}\left(|V_k| - |V_k^{\text{pre}}|\right) \times L_i \tag{35}$$

Here $|V_k|$ is the voltage magnitude corresponding to the collapse point for ΔS_i^N, and $|V_k^{\text{pre}}|$ are the voltage magnitudes related to the collapse point of ΔS_i^0. Whereas L_i is the imaginary part of a normalised right singular vector (i.e. $L = \Im(\boldsymbol{v}_n^0)$) that contains information about the sensitivity in the form of voltage magnitudes. Finally, one can solve the following system of equations to determine the margin of collapse for ΔS_i^N assuming that the right singular vector corresponding to null space of $\boldsymbol{J}^0$ is known.

$$f_i^N(x,\lambda) = 0, \quad i = 1,\ldots,n \tag{36a}$$

$$p_{\text{s}}(\boldsymbol{v}_n^0) = 0 \tag{36b}$$

The NC algorithm was formulated with either choice of parametric equations mentioned above. In the subsequent sections, a detailed computational perforce analysis is given.

6 Implementation

The implementation of the NC method is simple and easily programmable, as all the steps are similar to a traditional Newton–Raphson. Implementation was performed in Matlab using standard libraries from Matpower toolbox [52]. An academic version of the code is available at a public domain [53] for reproducing results from this paper and for further developments. Following machine configuration was used to produce all the results in this paper; Intel i7 with 16 Gb of RAM running at 2.8 GHz.

Fig. 2 shows a functional flowchart of the NC algorithm for better understanding the implementation. To update the margin to

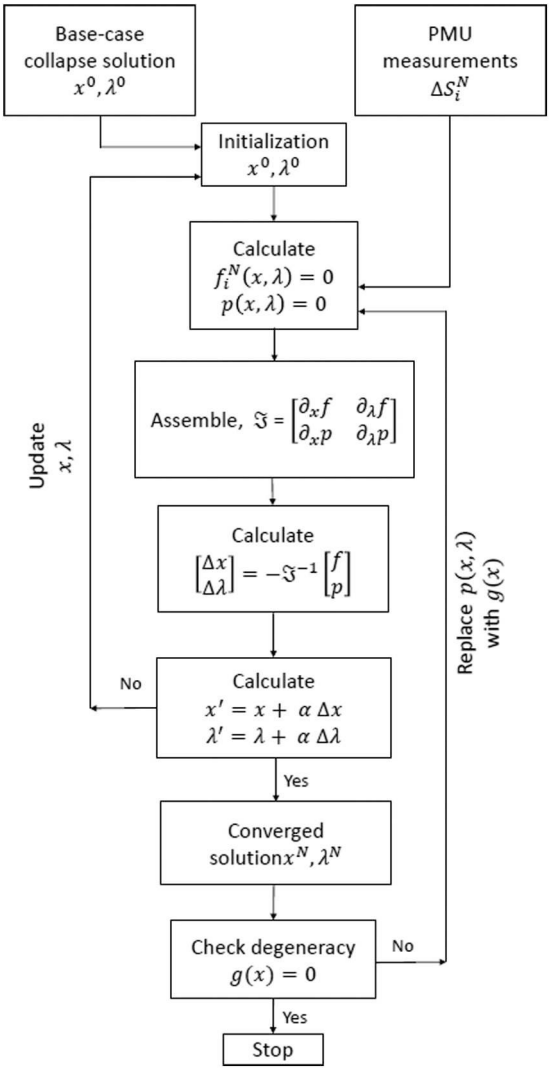

Fig. 2 *Flowchart of the NC algorithm*

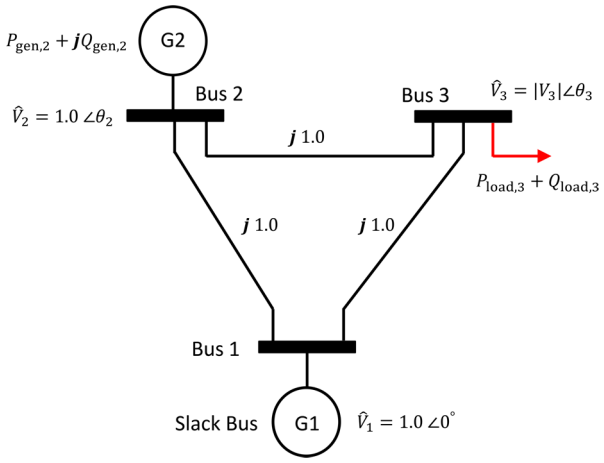

Fig. 3 *3-bus network*

collapse for given ΔS_i^N, the NC algorithm was formulated with three different parametric equations (i.e. p_{eig}, p_{svd}, and p_s). If x^0 and λ^0 represents a base-case collapse solution, then the following steps are performed such that the algorithm can always find a feasible solution.

i. First, information about new state ΔS_i^N is evaluated from the measurement devices.
ii. Then, NC iterations are initiated to compute the margin to collapse for ΔS_i^N with x^0 and λ^0 as an initial guess.
iii. Once the algorithm reaches a solution, i.e. x^N and λ^N, the degeneracy condition of $\boldsymbol{J}^N$ is checked through $g(x) = 0$.
iv. If the condition holds, then x^N and λ^N is the desired solution.
v. Otherwise, x^N and λ^N are set as an initial guess and iterations process is initiated by replacing $p(x, \lambda)$ equation with $g(x)$.

From the numerical experiments, it was observed that the algorithm found an accurate solution with the fast parameterisation techniques presented in this work. Results were obtained with four-digit precision.

7 Numerical studies

In the numerical experiments, several scenarios are devised to demonstrate the performance of the NC algorithm with either choice of parameterisation. In the numerical examples, the following setup was adopted:

i. First, a base-case regime ΔS_i^0 is defined, and then information about the non-trivial kernel of the base-case Jacobian (or simplify base-case collapse solution) is stored to be used in the NC iterations.
ii. While the continuously evolving operating state ΔS_i^N is assumed through rigorous assumptions. To represent a realistic view in terms of measurements, the state ΔS_i^N was given in terms of either change in power injections at some random buses or some significant changes in the network's topology (i.e. transmission line or generator outage, etc.). In some experiments, the assumed measurements were also subjected to random noise levels to depict the data quality issues from measurement devices.

But, in an actual practical environment, the online state ΔS_i^N monitoring takes into account two main factors; (i) the admittance matrix and (ii) voltage phasor measured at each bus. Usually, voltage magnitude and phase angle at each bus in a network are evaluated by the voltage phasor information available at PMU devices. Measurements from PMU goes through a pre-processing platform to assess the new operating state in terms of change in power injections and network topology [28]. However, PMUs are not placed at each node of an electric grid. To overcome this issue of insufficient observability, an adaptive state estimation algorithm is typically used to estimate the evolving operating regime by utilising the available PMUs data set [20, 28].

7.1 3-bus network

The proposed method is first applied to a small 3-bus system as shown in Fig. 3. Network configurations are as follows; bus 1 is a slack bus with voltage phasor $\hat{V}_1 = 1.0\angle 0°$. Bus 2 is treated as PV (generator) bus with voltage set point $\hat{V}_2 = 1.0\angle\theta_2$, while active and reactive power generations are denoted by $P_{gen,2}$ and $Q_{gen,2}$, respectively. Finally, bus 3 is a PQ (load) bus, the real and reactive loads at bus 3 are represented by $P_{load,2}$ and $Q_{load,2}$ with a complex voltage phasor denoted as $\hat{V}_3 = |V_3|\angle\theta_3$. All the lines in the network are lossless, the inductance was set to $X_{12} = X_{13} = X_{23} = 1.0$ p.u.

Based on the network settings, the power injection space is confined by $P_{gen,2}$, $P_{load,3}$ and $Q_{load,3}$. Whereas variable space consists of θ_2, θ_3 and $|V_3|$. The following general expressions describe the active power balance equations:

$$\sin\theta_2 + |V_3|\sin(\theta_2 - \theta_3) - \lambda(P_{gen,2}) = 0 \tag{37a}$$

$$|V_3|\sin\theta_3 + |V_3|\sin(\theta_3 - \theta_2) + \lambda(P_{load,3}) = 0 \tag{37b}$$

While the reactive power balance and the power flow Jacobian matrix (i.e. J) are described as

$$2|V_3|^2 - |V_3|\cos\theta_3 - |V_3|\cos(\theta_3 - \theta_2) + \lambda(Q_{\text{load},3}) = 0 \tag{38}$$

$$\boldsymbol{J} = \begin{bmatrix} J_{11} & J_{12} & J_{13} \\ J_{21} & J_{22} & J_{23} \\ J_{31} & J_{32} & J_{33} \end{bmatrix} \tag{39}$$

$$J_{11} = \cos\theta_2 + |V_3|\cos(\theta_2 - \theta_3) \tag{40a}$$

$$J_{12} = -|V_3|\cos(\theta_2 - \theta_3) \tag{40b}$$

$$J_{13} = \sin(\theta_2 - \theta_3) \tag{40c}$$

$$J_{21} = -|V_3|\cos(\theta_3 - \theta_2) \tag{40d}$$

$$J_{22} = |V_3|\cos\theta_3 + |V_3|\cos(\theta_3 - \theta_2) \tag{40e}$$

$$J_{23} = \sin\theta_3 + |V_2|\sin(\theta_3 - \theta_2) \tag{40f}$$

$$J_{31} = -|V_3|\sin(\theta_3 - \theta_2) \tag{40g}$$

$$J_{32} = |V_3|\sin\theta_3 + |V_3|\sin(\theta_3 - \theta_2) \tag{40h}$$

$$J_{33} = 4|V_3| - \cos\theta_3 - |V_2|\cos(\theta_3 - \theta_2) \tag{40i}$$

Here, we present a scenario constraining the $Q_{\text{load},3} = 0$, and calculate margin of voltage collapse/solvability boundary in space of $P_{\text{gen},2}$ and $P_{\text{load},3}$. A solid curve from Fig. 4 depicts the actual solvability boundary in $P_{\text{gen},2} - P_{\text{load},3}$ space, which was computed using the methodology from [10]. First, a base-case state ΔS_i^0 (see Fig. 4) is solved to find a point on the solvability boundary referred to as 'base-case collapse point'. The information about such solution point is saved to be used as an initialisation in the NC iterations. From base-case collapse solution, details about eigenvectors ($\boldsymbol{y}^0$ and $\boldsymbol{z}^0$) and singular vectors ($\boldsymbol{u}_n^0$ and $\boldsymbol{v}_n^0$) corresponding to the null space of $\boldsymbol{J}^0$ are also saved.

In order to simulate an online scenario, we discretise $P_{\text{gen},2} - P_{\text{load},3}$ grid as follows. $P_{\text{load},3} = R\cos\phi$ and $P_{\text{gen},2} = R\sin\phi$ with $R = 0.2$ and $0 \le \phi \le (\pi/4)$. Each discretise direction in $P_{\text{gen},2}P_{\text{load},3}$ plane represents a new operating regime ΔS_i^N, which was solved using the NC algorithm with the proposed choices of $p(x, \lambda)$. From Fig. 4, it can be seen that the algorithm calculates the points in a close proximity to the actual solvability boundary with either choices of parameterisation, i.e. p_{eig}, p_{svd}, and p_{s}. Also, the NC algorithm converged quadratically with less than ten iterations. No such case was observed in which the proposed parameterisation failed to find a correct solution. This example confirms the precision and convergence of the algorithm.

The next section presents details about different IEEE networks with some practical scenarios.

7.2 IEEE 14-bus network

In this section, an IEEE 14-bus test network [54] is analysed. The network structure consists of four PV buses, nine PQ buses, and bus one as a slack bus. Several practical scenarios are considered to assess the performance, robustness and numerical instabilities encountered by the NC algorithm for different choices of parametric equations, i.e. p_{eig}, p_{svd}, and p_{s}. For simplicity, the base-case regime ΔS_i^0 was based on the power injections provided in the Matpower data file [52]. For ΔS_i^0, the margin of voltage collapse was $\lambda^0 = 4.060$.

The small disturbance: In the normal operation, the state of the network changes due to small variations like load increase or decrease at certain buses. Therefore, the new state of the network ΔS_i^N can be viewed as a perturbed base-case state. To simulate an online mode, ΔS_i^N was defined as follows:

$$\Delta S_i^N = \sigma_j \Delta S_i^0. \tag{41}$$

such that

$$\sigma_j = \begin{cases} 1 & \text{if } i \ne j \\ \eta & \text{otherwise} \end{cases} \tag{42}$$

Here, index i describes the number of buses in the network, while index j corresponds to the perturbed buses where power injections are varied by an amount η. Normally, the selection of perturbed buses is made from real-time measurement.

- In the first case, the power injections at the following buses are perturbed $\mathbb{L} = \{5, 7, 13\}$. At these buses, the power injections were gradually increased up to 60%. The summary of this case is shown in Table 1. Here, λ_{eig}, λ_{svd}, and λ_{s} define the margin of voltage collapse obtained from the NC algorithm for p_{eig}, p_{svd}, and p_{s}, respectively. And λ_{CPF} in the table represents the actual distance to the voltage collapse obtained from CPF solver proposed in [21]. From Table 1, it is clear that the difference between λ_{s} obtained from the NC algorithm with either choices of $p(x, \lambda)$ and λ_{CPF} is less than 1%. Therefore, confirms the precision of the obtained results.
- The second case considers some other random buses, i.e. $\mathbb{L} = \{9, 11, 14\}$. The amount of maximum power injections perturbation at these buses was 80%. Results from Table 1 show that the algorithm converged with relatively small error.
- A third case selects $\mathbb{L} = \{3, 13, 14\}$ with maximum perturbation amount up to 90%. The precision of the results was similar to the previous cases.

For each case, the proposed parameterisation worked well, and the NC algorithm reached a solution within ten iterations. Numerical results also confirm that the choice of buses and level of power injection variation did not affect the performance of the algorithm.

Time domain simulations: In the time-domain simulations, several examples are explored. To portray a realistic picture, in given scenarios, power injections at random buses are perturbed over a time interval with either fixed or variable fluctuations. Results are presented from a time frame $t \in [0 \quad 240]$ s. Here, $t = 0$ s corresponds to a base-case state defined by the initial power injections, while $t = 240$ s denotes the maximum allowable power injection state.

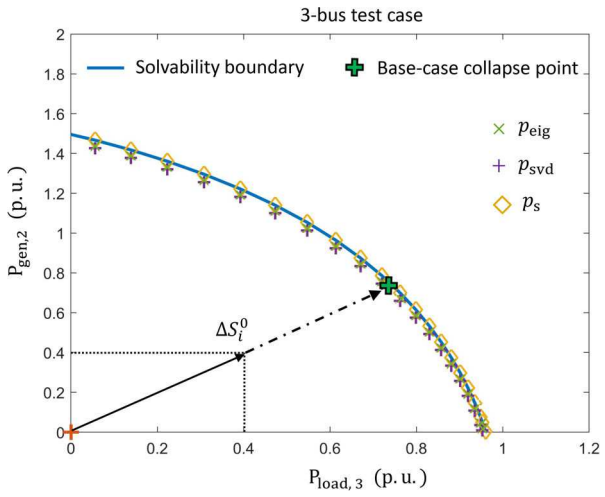

Fig. 4 *Solvability boundary in $P_{\text{gen},2} - P_{\text{load},3}$ space*

Table 1 Summary for IEEE 14-bus case (small disturbances)

Cases	$\mathbb{L}$	λ_{eig}	λ_{svd}	λ_{s}	λ_{CPF}
01	5,7,13	3.812	3.812	3.811	3.813
02	9,11,14	2.923	2.922	2.924	2.926
03	3,13,14	2.801	2.800	2.776	2.803

• *Case 1:* The active power injection at load buses 4, 5, 12, 13, and 14 is gradually increased after every 2 s with a ± 20% fixed variations. The values of λs obtained in this scenario are shown in Fig. 5 with a blue curve. Here, the fluctuations in the curves represent the noise level from measurement devices.
• *Case 2:* Unlike in the previous example, here the active power injection at following buses 4, 9, 10, 11, and 13, is gradually ramped up every 2 s. And after every 10 s,, a random noise level was added, ranging from ±10 to ±50%. The computed values of λ_s are shown by a red curve in Fig. 5.

For both cases, the growth of active power injections over time is depicted in Figs. 6 and 7, respectively. In either case, at each time interval, the NC algorithm converged quadratically (i.e. less than ten iterations) with a higher degree of precision.

The large disturbance: In the case of large disturbances, the system tries to maintain steady voltages following disturbances like system faults, transmission line tripping, generation outages, or other circuit contingencies [9]. For practical purposes, scenarios are considered to analyse the performance of the NC algorithm with different choices of $p(x, \lambda)$.

• In the first case, a line outage is simulated between buses 2 and 4 such that the network connectivity is preserved. Also, the power injections at each bus were kept the same as in the base-case. Values of λ's obtained for each choice of parametric equations are provided in Table 2. Results obtained from the NC algorithm are close to the actual solution.
• In the second case, line outages are considered between buses 2 and 4, and also between buses 4 and 9. It's noticeable from Table 2 that the precision of results is still quite high.
• The last case considers three line outages. An addition to the previous line outages the transmission line between buses 2 and 5 is also tripped along with a generator outage at bus 2. From Table 2, it is observable that for p_{eig} and p_{svd}, the NC method reached to a close value of λ_{CPF}. However, the parameterisation choice based on p_s the solution was a bit far from the λ_{CPF}. To avoid such situation, the NC iterations are started again by replacing p_s with a transversality condition $g(x)$. And previously obtained solution is used an initial guess to keep the computational time minimum.

7.3 Computational performance

In this section, results for various IEEE test cases are presented to evaluate the computational performance of the NC algorithm. First, the precision of the algorithm was determined with the proposed choices of parametric equations. In Table 3, the algorithm was initiated to solve several IEEE test networks ranging from small to large. To simulate an online scenario for ΔS_i^N, the standard base-case regime was perturbed by increasing active and reactive power injections up to 50% at some random buses. The choice of such buses is denoted by $\mathbb{L}$ in Table 3. Whereas λ_{eig}, λ_{svd} and λ_s correspond to the margin of voltage collapse for p_{eig}, p_{svd} and p_s, respectively. And λ_{CPF} related to the actual distance to voltage collapse obtained from the CFP solver [21]. It can be observed from Table 3 that for different choices of parametric equations, the relative error between computed values of λs and λ_{CPF} is less than 1%.

The results in Table 4 discuss the convergence of algorithm with different parametric equations. These results correspond to scenario considered in Table 3. Here τ_{eig}, τ_{svd} and τ_s describe the number of Newton iterations required to reach the solution for p_{eig}, p_{svd} and p_s, respectively. It is evident from Table 4, the NC algorithm with either choice of the parametric equations converges within 10 or 11 iterations. The overall convergence the algorithm is quadratic but the choice of p_{svd} resulted in a small number of iterations in comparison to p_{eig} and p_s.

Finally, the computational speed and scalability to the large test cases was assessed. In Table 5, t_{eig}, t_{svd} and t_s represent the total time required to reach a solution for p_{eig}, p_{svd} and p_s, respectively.

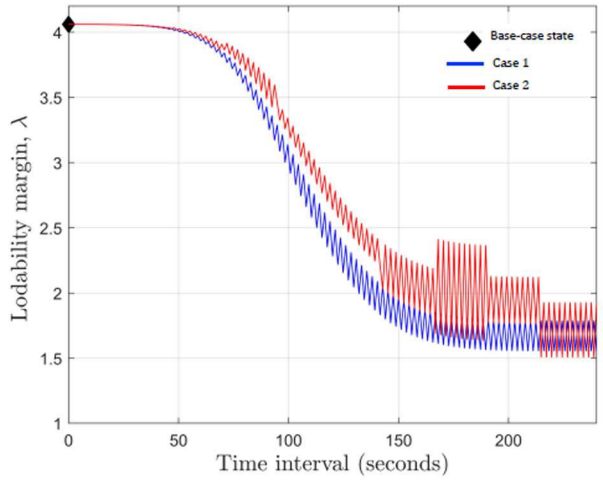

Fig. 5 *Updated loadability margins (λ) over time*

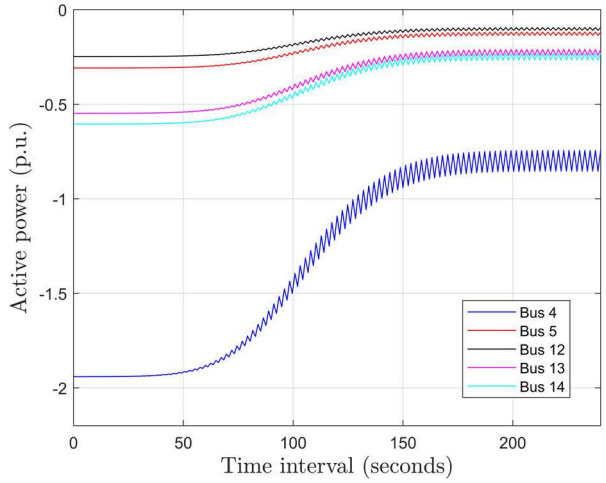

Fig. 6 *Case 1: growth of active power injections over time*

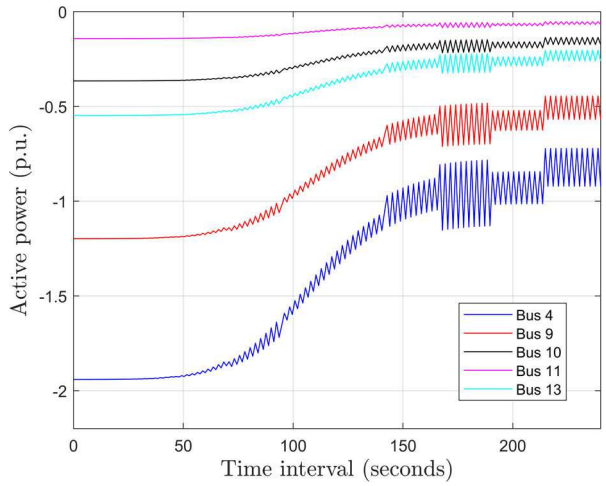

Fig. 7 *Case 2: growth of active power injections over time*

Table 2 Summary for IEEE 14-bus case (large disturbances)

Cases	λ_{eig}	λ_{svd}	λ_s	λ_{CPF}
01	3.278	3.279	3.251	3.302
02	3.249	3.249	3.213	3.267
03	2.292	2.290	2.289	2.293

While t_{CPF} corresponds to the time for the CPF algorithm. The overall computational time for the NC algorithm is very small and comparable to even normal power flow solver. Although the

Table 3 Summary for different IEEE cases

IEEE cases	$\mathbb{L}$	λ_{eig}	λ_{svd}	λ_{s}	λ_{CPF}
14 bus	5, 7, 13, 14	3.579	3.581	3.583	3.584
30 bus	3, 5, 14, 16, 29	2.759	2.760	2.761	2.761
57 bus	5, 10, 13, 56, 57	1.832	1.833	1.830	1.833
118 bus	11, 13, 60, 75, 90	2.967	2.969	2.965	2.969
300 bus	3, 8, 90, 91, 297	1.426	1.425	1.427	1.429
2383 bus	1000, 2370, 2380 2381, 2382, 2383	1.885	1.886	1.882	1.886

Table 4 Number of iterations for different IEEE cases

IEEE cases	τ_{eig}	τ_{svd}	τ_{s}
14 bus	8	6	10
30 bus	7	6	9
57 bus	9	5	10
118 bus	9	5	11
300 bus	8	5	11
2383 bus	9	7	10

Table 5 Computational time for different IEEE cases

IEEE cases	t_{eig}, s	t_{svd}, s	t_{s}, s	t_{CPF}, s
14 bus	0.0038	0.0030	0.0028	1.1650
30 bus	0.0048	0.0031	0.0039	4.0093
57 bus	0.0070	0.0044	0.0068	5.4375
118 bus	0.0112	0.0056	0.0109	8.3893
300 bus	0.0202	0.0102	0.0211	8.4501
2383 bus	0.2073	0.1630	0.2314	12.740

computational speed among each parametric choice is comparable but condition based on the p_{svd} surpasses the others due to a small number of iterations.

To summarise, the proposed algorithm provides a fast way to update the distance to voltage collapse in real-time for each new state of the network. The algorithm can also presents the precise results with tractability to large networks.

8 Conclusions and future work

The paper proposes a novel method for the online voltage stability assessment referred to as the 'Newton-Corrector' algorithm. The algorithmic procedure updates the margin of collapse for a continuously evolving state of a network without significant computational effort. This is done by utilising the base-case collapse point and incoming measurements. The NC algorithm offers several advantages over the traditional approaches to this problem. First, unlike in index-based methodologies, it provides a quantitative measure of distance to voltage collapse. Second, the algorithm does not require a re-formulated power flow model. Thus the implementation is straightforward. Third, it solves a set of power flow equations supplemented by just one scalar auxiliary condition; therefore, the computational burden of each iteration is comparable to a traditional power flow analysis. Finally, it is worth noticing that initialisation does not require solving for some null space eigenvectors.

The algorithm's underlying mathematical structure uses a parametric equation formulated from a base-case collapse point solution. Although there are several ways to express this condition, this paper presents three versions, i.e. p_{eig}, p_{svd}, and p_{s} based on the non-trivial kernel of a base-case Jacobian. From detailed numerical experimentation, it was observed that p_{svd} equation transcends the other choices in terms of the number of iterations, numerical stability, robustness, and scalability. This paper also covers detailed performance analysis and comparison of the proposed parametric conditions, together with the clear conclusions concerning the best option.

In numerical studies, several practical cases are considered to represent a realistic scenario. From all the numerical experiments, it was observed that the NC algorithm with either choice of parameterisation finds an accurate solution and does not encounter any numerical stability issues. From the context of future studies, there are numerous possible extensions to this method: examining more practical scenarios and extending the current formulation to investigate the effects of transient voltage stability. And finally, using the NC algorithm to calculate nomograms of the power flow solution space.

9 Acknowledgments

The authors thank Prof. Janusz Bialek from the Center for Energy Science & Technology (CEST) at the Skolkovo Institute of Science and Technology for his support and guidance.

10 References

[1] Löf, P., Smed, T., Andersson, G., *et al.*: 'Fast calculation of a voltage stability index', *IEEE Trans. Power Syst.*, 1992, **7**, (1), pp. 54–64

[2] Van Cutsem, T., Vournas, C.: '*Voltage stability of electric power systems*', vol. **441** (Springer, Germany, 1998)

[3] Diao, R., Sun, K., Vittal, V., *et al.*: 'Decision tree-based online voltage security assessment using pmu measurements', *IEEE Trans. Power Syst.*, 2009, **24**, (2), pp. 832–839

[4] Moghavvemi, M., Omar, F.: 'Technique for contingency monitoring and voltage collapse prediction', *IEE Proc., Gener. Transm. Distrib.*, 1998, **145**, (6), pp. 634–640

[5] Canizares, C.A., Dobson, I., Van Cutsem, T., *et al.*: 'Voltage stability assessment: concepts, practices and tools'. IEEE/PES Power System Stability Subcommittee Special Publication (SP101PSS), USA, 2002

[6] Maharjan, R., Kamalasadan, S.: 'Voltage stability index for online voltage stability assessment'. North American Power Symp. (NAPS), Charlotte, North Carolina, USA, 2015, pp. 1–6

[7] Kwatny, H., Pasrija, A., Bahar, L.: 'Static bifurcations in electric power networks: loss of steady-state stability and voltage collapse', *IEEE Trans. Circuits Syst.*, 1986, **33**, (10), pp. 981–991

[8] Sauer, P.W., Pai, M.: 'Power system steady-state stability and the load-flow jacobian', *IEEE Trans. Power Syst.*, 1990, **5**, (4), pp. 1374–1383

[9] Kundur, P., Paserba, J., Ajjarapu, V., *et al.*: 'Definition and classification of power system stability IEEE/CIGRE joint task force on stability terms and definitions', *IEEE Trans. Power Syst.*, 2004, **19**, (3), pp. 1387–1401

[10] Hiskens, I.A., Davy, R.J.: 'Exploring the power flow solution space boundary', *IEEE Trans. Power Syst.*, 2001, **16**, (3), pp. 389–395

[11] Ajjarapu, V.: '*Computational techniques for voltage stability assessment and control*' (Springer Science & Business Media, Germany, 2007)

[12] Ali, M., Dymarsky, A., Turitsyn, K.: 'Transversality enforced newton raphson algorithm for fast calculation of maximum loadability', *IET. Gener. Transm. Distrib.*, 2018, **12**, (8), pp. 1729–1737

[13] Chiang, H.-D., Dobson, I., Thomas, R.J., *et al.*: 'On voltage collapse in electric power systems', *IEEE Trans. Power Syst.*, 1990, **5**, (2), pp. 601–611

[14] Van Cutsem, T., Moisse, C., Mailhot, R.: 'Determination of secure operating limits with respect to voltage collapse', *IEEE Trans. Power Syst.*, 1999, **14**, (1), pp. 327–335

[15] Abe, S., Fukunaga, Y., Isono, A., *et al.*: 'Power system voltage stability', *IEEE Trans. Power Appar. Syst.*, 1982, **10**, pp. 3830–3840

[16] Carreras, B.A., Newman, D.E., Dobson, I., *et al.*: 'Evidence for self-organized criticality in a time series of electric power system blackouts', *IEEE Trans. Circuits Syst. I, Regul. Pap.*, 2004, **51**, (9), pp. 1733–1740

[17] Dobson, I., Carreras, B.A., Lynch, V.E., *et al.*: 'Complex systems analysis of series of blackouts: cascading failure, critical points, and self-organization', *Chaos: An Interdisciplinary J. Nonlinear Sci.*, 2007, **17**, (2), p. 026103

[18] LÖf, P.-A., Hill, D.J., Arnborg, S., *et al.*: 'On the analysis of long-term voltage stability', *Int. J. Electr. Power Energy Syst.*, 1993, **15**, (4), pp. 229–237

[19] Lof, P.-A., Andersson, G., Hill, D.: 'Voltage stability indices for stressed power systems', *IEEE Trans. Power Syst.*, 1993, **8**, (1), pp. 326–335

[20] Glavic, M., Van Cutsem, T.: 'Wide-area detection of voltage instability from synchronized phasor measurements. part I: principle', *IEEE Trans. Power Syst.*, 2009, **24**, (3), pp. 1408–1416

[21] Ajjarapu, V., Christy, C.: 'The continuation power flow: a tool for steady state voltage stability analysis', *IEEE Trans. Power Syst.*, 1992, **7**, (1), pp. 416–423

[22] Avalos, R.J., Cañizares, C.A., Milano, F., *et al.*: 'Equivalency of continuation and optimization methods to determine saddle-node and limit-induced bifurcations in power systems', *IEEE Trans. Circuits Syst. I, Regul. Pap.*, 2009, **56**, (1), pp. 210–223

[23] Rao, S.D., Tylavsky, D.J., Feng, Y.: 'Estimating the saddle-node bifurcation point of static power systems using the holomorphic embedding method', *Int. J. Electr. Power Energy Syst.*, 2017, **84**, pp. 1–12

[24] Gao, B., Morison, G., Kundur, P.: 'Voltage stability evaluation using modal analysis', *IEEE Trans. Power Syst.*, 1992, **7**, (4), pp. 1529–1542

[25] Morison, G., Gao, B., Kundur, P.: 'Voltage stability analysis using static and dynamic approaches', *IEEE Trans. Power Syst.*, 1993, **8**, (3), pp. 1159–1171

[26] Grainger, J.J., Stevenson, W.D., Stevenson, W.D., *et al.*: 'Power system analysis', 2003

[27] Canizares, C.A., De Souza, A.C., Quintana, V.H.: 'Comparison of performance indices for detection of proximity to voltage collapse', *IEEE Trans. Power Syst.*, 1996, **11**, (3), pp. 1441–1450
[28] Balamourougan, V., Sidhu, T., Sachdev, M.: 'Technique for online prediction of voltage collapse', *IEE Proc., Gener. Transm. Distrib.*, 2004, **151**, (4), pp. 453–460
[29] Bao, L., Huang, Z., Xu, W.: 'Online voltage stability monitoring using var reserves', *IEEE Trans. Power Syst.*, 2003, **18**, (4), pp. 1461–1469
[30] Corsi, S.: '*Voltage control and protection in electrical power systems: from system components to wide-area control*' (Springer, Germany, 2015)
[31] Begovic, M.M., Phadke, A.G.: 'Control of voltage stability using sensitivity analysis', *IEEE Trans. Power Syst.*, 1992, **7**, (1), pp. 114–123
[32] Sinha, A., Hazarika, D.: 'A comparative study of voltage stability indices in a power system', *Int. J. Electr. Power Energy Syst.*, 2000, **22**, (8), pp. 589–596
[33] Capitanescu, F., Van Cutsem, T.: 'Unified sensitivity analysis of unstable or low voltages caused by load increases or contingencies', *IEEE Trans. Power Syst.*, 2005, **20**, (1), pp. 321–329
[34] Gubina, F., Strmcnik, B.: 'Voltage collapse proximity index determination using voltage phasors approach', *IEEE Trans. Power Syst.*, 1995, **10**, (2), pp. 788–794
[35] Vu, K., Begovic, M.M., Novosel, D.*, et al.*: 'Use of local measurements to estimate voltage-stability margin', *IEEE Trans. Power Syst.*, 1999, **14**, (3), pp. 1029–1035
[36] Julian, D., Schulz, R.P., Vu, K.*, et al.*: 'Quantifying proximity to voltage collapse using the voltage instability predictor (vip)'. 2000 Power Engineering Society Summer Meeting (Cat. No. 00CH37134), Seattle, Washington, USA, 2000, vol. 2, pp. 931–936
[37] Verbič, G., Gubina, F.: 'Fast voltage-collapse line-protection algorithm based on local phasors', *IEE Proc., Gener. Transm. Distrib.*, 2003, **150**, (4), pp. 482–486
[38] Smon, I., Verbic, G., Gubina, F.: 'Local voltage-stability index using tellegen's theorem', *IEEE Trans. Power Syst.*, 2006, **21**, (3), pp. 1267–1275
[39] Liu, J.-H., Chu, C.-C.: 'Wide-area measurement-based voltage stability indicators by modified coupled single-port models', *IEEE Trans. Power Syst.*, 2013, **29**, (2), pp. 756–764
[40] Kamalasadan, S., Thukaram, D., Srivastava, A.: 'A new intelligent algorithm for online voltage stability assessment and monitoring', *Int. J. Electr. Power Energy Syst.*, 2009, **31**, (2–3), pp. 100–110
[41] Zhou, D.Q., Annakkage, U.D., Rajapakse, A.D.: 'Online monitoring of voltage stability margin using an artificial neural network', *IEEE Trans. Power Syst.*, 2010, **25**, (3), pp. 1566–1574
[42] Trias, A.: 'The holomorphic embedding load flow method'. 2012 IEEE Power and Energy Society General Meeting, San Diego, California, USA, 2012, pp. 1–8
[43] Liu, C., Wang, B., Hu, F.*, et al.*: 'Online voltage stability assessment for load areas based on the holomorphic embedding method', *IEEE Trans. Power Syst.*, 2018, **33**, (4), pp. 3720–3734
[44] Ayuev, B.I., Davydov, V.V., Erokhin, P.M.: 'Fast and reliable method of searching power system marginal states', *IEEE Trans. Power Syst.*, 2016, **31**, (6), pp. 4525–4533
[45] Leonardi, B., Ajjarapu, V.: 'Development of multilinear regression models for online voltage stability margin estimation', *IEEE Trans. Power Syst.*, 2010, **26**, (1), pp. 374–383
[46] Morison, K., Wang, L., Kundur, P.: 'Power system security assessment', *IEEE Power Energy Mag.*, 2004, **2**, (5), pp. 30–39
[47] Overbye, T.J.: 'Computation of a practical method to restore power flow solvability', *IEEE Trans. Power Syst.*, 1995, **10**, (1), pp. 280–287
[48] Ejebe, G., Wollenberg, B.: 'Automatic contingency selection', *IEEE Power Appar. Syst.*, 1979, **PAS-98**, (1), pp. 97–109
[49] Ali, M., Gryazina, E., Turitsyn, K.S.: 'Methodology for computation of online voltage stability assessment'. 2018 IEEE Int. Conf. on Environment and Electrical Engineering and 2018 IEEE Industrial and Commercial Power Systems Europe (EEEIC/I&CPS Europe), Palermo, Italy, 2018, pp. 1–5
[50] Abbott, J.P.: 'An efficient algorithm for the determination of certain bifurcation points', *J. Comput. Appl. Math.*, 1978, **4**, (1), pp. 19–27
[51] Tate, J.E., Overbye, T.J.: 'A comparison of the optimal multiplier in polar and rectangular coordinates', *IEEE Trans. Power Syst.*, 2005, **20**, (4), pp. 1667–1674
[52] Zimmerman, R.D., Murillo-Sanchez, C.E., Thomas, R.J.: 'MATPOWER: steady-state operations, planning, and analysis tools for power systems research and education', *IEEE Trans. Power Syst.*, 2011, **26**, (1), pp. 12–19
[53] Ali, M.: 'Matlab Implementation of Newton-Corrector Algorithm', 2019. Available at https://github.com/mazharalipak/Newton-corrector
[54] Christie, R.: 'Power systems test case archive'. Electrical Engineering Dept., University of Washington, 2000